Submitted: 2025-07-25 Accepted: 2026-02-03 Published: 2026-07-21

OZeAN
Online Zeitschrift zur Antiken Numismatik

Issue 8 (2026) pp. 17–36

Measurement of the chemical composition of ancient coins with portable XRF

by Malte Overkemping, Sven Lemke, Stephanie Lindner, Gregor Staab and Erik Strub

DOI 10.17879/ozean-2026-10056

Contact: Malte Overkemping, Sven Lemke and E. Strub*: University of Cologne, Division of Nuclear Chemistry, Zülpicher Str. 45, D - 50674 Köln, Germany

Stephanie Lindner and Gregor Staab: University of Cologne, Department of Classics, Albertus-Magnus-Platz, D - 50923 Köln, Germany

*corresponding author: erik.strub@uni-koeln.de

Edited on behalf of the Forschungsstelle Antike Numismatik at Münster University
by Stefan Krmnicek, Achim Lichtenberger and Katharina Martin
ozean-numismatik.de / ISSN 2690-4490
Published with support of the Numismatische Kommission der Länder in der Bundesrepublik Deutschland

Measurement of the chemical composition of ancient coins with portable XRF

Malte Overkemping, Sven Lemke, Stephanie Lindner, Gregor Staab und Erik Strub

Abstract: The elemental composition of antique coins is of great interest in the field of numismatics. An obvious quick and easy method to investigate these artifacts is X-Ray fluorescence, especially using portable spectrometers, although these spectrometers are limited in terms of precision and accuracy of the measurement results. In this work some shortcomings of XRF spectrometry were investigated. A crucial point is that enough single measurements should be taken to obtain meaningful averaged elemental compositions, leading to an increase in precision. Further, correction factors were derived to improve accuracy, so that overall, the set of data will be improved regarding both precision and accuracy. These correction factors were based either on reference samples or on simulations, thus demonstrating the feasibility of deriving meaningful correction parameters for defined sets of coins. Although portable XRF can possibly not replace high-precision/high accuracy measurements like ICP-MS, we show that nevertheless results, especially when obtained from a set of samples and from multiple measurements of one and the same sample, can be used to differentiate the material nature of uniform groups of coins, e.g. to find correlations between trace element concentrations or to identify clusters. Thus, portable XRF provides easy access to measurement of high sample numbers with the potential to discover yet unknown trends in composition, e.g. in numismatic collections.

Keywords: X-ray fluorescence spectrometry (XRF), XRF correction factors, XRF simulations, surface roughness, Roman billon coins, lead-bronze coins

Zusammenfassung: Die elementare Zusammensetzung antiker Münzen ist in der Numismatik von großem Interesse. Eine einfache und schnelle Methode ist die Röntgenfluoreszenzspektrometrie, besonders mit portablen Geräten, wobei die Genauigkeit und Richtigkeit der Resultate limitiert sind. Einige dieser Limitierungen wurden in dieser Arbeit genauer untersucht. Um aussagekräftige gemittelte Elementkonzentrationen zu bestimmen, sollte die Zahl der Einzelmessungen groß gewählt werden. Eine höhere Genauigkeit der Daten lässt sich generell durch eine höhere Anzahl an Einzelmessungen erreichen. Durch Korrekturfaktoren lässt sich auch die Richtigkeit verbessern; diese wurden in dieser Arbeit über zwei verschiedene Herangehensweisen ermittelt. Zunächst wurde ein Korrekturfaktor über Referenzproben mit bekannter Elementkonzentration ermittelt. Anschließend wurde ein weiterer Korrekturfaktor über ein Simulationsprogramm bestimmt. Die Röntgenfluoreszenzspektrometrie kann mithilfe dieser Korrekturfaktoren insgesamt richtigere und präzisere Messwerte liefern, wird jedoch hochpräzise und richtige Methoden, wie ICP-MS, nicht ersetzen können. Die Möglichkeit, viele Einzelmessungen in kurzer Zeit durchzuführen, erhöht aber die Präzision und die Korrekturfaktoren erhöhen die Richtigkeit der Datensätze. Insgesamt ist dies hinreichend für eine Untersuchung von einheitlichen Münzgruppen, z. B. im Hinblick Korrelationen von Spurenelementen mit Hauptkomponenten. Damit bietet die portable Röntgenspektrometrie einen einfachen Zugang zur Messung großer Münzgruppen und die Möglichkeit, bisher unbekannte Trends in Zusammensetzungen zu finden.

Stichworte: Röntgenfluoreszenzspektrometrie (XRF), XRF-Korrekturfaktoren, XRF Simulationen, Oberflächenrauheit, römische Billonmünzen, Bleibronze-Münzen

1. Introduction

1.1. Methods for elemental analysis of historical artifacts

In archaeology many different characteristics of an artifact are of interest. One of these characteristics is the elemental composition of artifacts, which is the concentration of the chemical elements within the artifact. Knowledge of element composition can help assign the sample to a specific era or provide information about the provenience, production methods, or raw materials use[1]. In general, such an elemental analysis might be performed with destructive, semi-destructive and non-destructive methods. Using destructive analytical methods, a sample is consumed during the measurement process. However, the size of the sample may be very small, so that only minor damage needs to be inflicted on the artifact. Central concepts for the comparison of different analytical methods are accuracy and precision of measurements are of great interest (see **figure 1**).

Some analytical methods deliver both precise and accurate data, some are only yielding either precise or accurate data, and some methods are limited in both precision and accuracy. Destructive methods like inductively coupled plasma mass spectrometry (ICP-MS)[2] or inductively coupled plasma optical emission spectroscopy (ICP-OES)[3] can very precisely determine the elemental composition of the sample, based on sample sizes in mg or even in the sub-mg range[4]. With a suitable calibration, these measurements will also provide high accuracy. With a laser coupled to the spectrometer, laser-ablation inductively coupled plasma mass spectrometry (LA-ICP-MS)[5], samples can e.g. be taken from a small spot of a historical artifact with a diameter of less than 0.1 mm and only a few µm deep. In this sense, LA-ICP-MS might be called ›semi-destructive‹ as such a spot is barely visible to the naked eye on a bigger artifact. Nevertheless, the artifact is not unharmed in a strict sense, so curators might remain skeptical of such a method. LA-

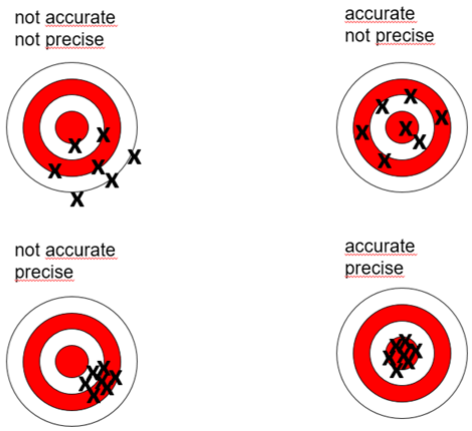

Figure 1: Representation of the difference between precision and accuracy

ICP-MS needs no chemical sample treatment and therefore consecutive measurements can be made in short time, but its use remains limited due to the fact than an LA-ICP-MS is not a portable instrument. Artifacts that are to be measured must be brought in a scientific lab and despite its virtual non-destructiveness, decisions of collection curators are needed to prevent or mitigate unnecessary influence on the artifacts. Although environments do exist, that foster such close relationships between humanities and scientists as the CRNS lab collaborating with the Louvre museum[6], this is rather an exemption. On the other hand, there is a broad range of spectroscopic techniques that are in general non-destructive, e.g. nuclear magnetic resonance (NMR)[7], infrared spectroscopy (IR)[8], as well as X-ray fluorescence (XRF)[9], that are all radiation based and have been successfully ap-

1 Zmuda-Trzebiatowska et al. 2019; Van Ham-Meert et al. 2020; Mozgai et al. 2021; Wallace et al. 2021, 343–371.
2 Houk et al. 1980, 2283–2289.
3 Boumans – Vrakking 1987a, 819–840; Boumans – Vrakking 1987b, 553–579; Boumans – Vrakking 1987c, 513–525.
4 Kusko et al. 1990, 49. 288–292.
5 Jarvis – Williams 1993, 251–262.
6 Kusko et al. 1990, 49. 288–292.
7 Proctor – Yu 1950, 717–717.
8 Pimentel 1960, 651.
9 Hoyo-Meléndez 2017, 257–262.

plied to historical artifacts. All these methods can be highly precise and have the potential for high accuracy, if calibrated. Also, Neutron activation analysis (NAA)[10] can be classified as a non-destructive method. Although NAA might lead to an activation of the sample during the investigation (i.e. the generation of a small amount of temporary or permanent radioactivity), the method has been used successfully multiple times[11]. One advantage of NAA is that it can be calibrated relatively easily because matrix effects in the calibration are mostly negligible. Of the different spectroscopic methods, XRF is to be highlighted: XRF can deliver the elemental composition of a sample in a non-destructive way, there is a broad experience analysis of artifacts with different X-ray sources[12] and second, small portable XRF spectrometers that can be used within the museum context are available for several years[13]. In these devices, a small X-ray tube is used to irradiate the sample, and the equipment is small and light enough to place it on a simple tripod in any orientation. Hence it can be applied as well as to artifacts of any size or paintings without even moving them out of an exhibition environment. However, especially portable XRF is limited in both accuracy and precision, because both might be influenced by the sample geometry (e.g. surface structure and roughness). Generally, X-ray fluorescence might also be induced using a particle beam (PIXE, for particle induced X-ray-emission)[14] or the strong radiation of a synchrotron source[15]: Both methods can be advantageous under different circumstances but are not portable.

However, the limitations of XRF that might hamper widespread use are:

1. XRF works better with heavier chemical elements, i.e. it is not well-suited for the analysis of the main components of organic materials,
2. possible matrix effects influence the accuracy of the results, i.e. the accuracy might decrease, especially if the object contains multiple chemical elements,
3. measurement results, especially precision, might be influenced by the sample surface geometry, as will be explained in more detail below,
4. XRF is generally not a high accuracy method, also depending on the sample composition,
5. measuring depth and width are limited, giving inconclusive results in the case of inhomogeneous materials.

With this work we want to show that XRF can be successfully applied when

1. light chemical elements play no role (like in metal alloys),
2. matrix effects can be minimized using suitable calibration methods,
3. the influence of sample geometry can be estimated by a model,
4. high accuracy is not decisive e.g. for analyzing groups of artifacts, i.e. when several subsets of samples are compared to each other,
5. when enough measurement points are used, yielding a representative (and thus more precise) composition for a single object and allowing for a statistical approach when several samples are measured.

We will demonstrate this throughout this paper on the example of ancient Alexandrian coins from the Roman period, lead-bronze coins (drachms) and billon coins (tetradrachms) of Claudius (41–54 AD) and Nero (54–68 AD). We will explicitly show how some of the limitations of XRF can be overcome when measurements

[10] Greenberg et al. 2011, 193–207.
[11] Gordus et al. 1967, 87–96.
[12] Guerra et al. 2008, 2334–2338; Reiche et al. 2004, 83–91; Alfeld 2020, 72–75; Vittiglio et al. 1999, 1697–1710.
[13] Shackley 2011, 1–6.
[14] Johansson 1989, 48–53; Malmqvist et al. 1989, 685–689; Johansson 1990, 167–188.
[15] Guerra et al. 2008, 2334–2338; Reiche et al. 2004, 83–91.

on a larger group of coins (n = 20) are performed and analyzed, revealing new information. We will show that accuracy as well as precision can be improved by making use of correction factors and a large number of single measurements for each coin. While this does not overcome completely the limitations of portable XRF, with these procedures data gained from large sample sets (e.g. of coins) might discover yet unknown trends and provide new insights.

1.2. Aim of this work

In this work, we describe how the influence of self-absorption on XRF-spectra can be corrected by introducing a correction factor (improving mostly accuracy) and how the influence of patina and surface effects can be minimized with multiple measurements (improving precision). Self-absorption correction factors were obtained in two different ways: for lead-bronze coins, we produced and measured artificial reference samples; for billon coins we simulated different coins with the program XMI-MSIM[16]. The correction factors obtained were applied to the measured data of the coins. XMI-MSIM was also used to estimate measurement uncertainties resulting from geometrical effects (like embossment).

By these simulations it is underpinned that the uncertainties resulting from patina or surface effects are consistent with the statistical uncertainty obtained from multiple measurements. In contrast to the use of references samples, simulations with XMI-MSIM are more versatile. Finally, some actual results from the measurement of the different coins are discussed.

1.3. Principles, Possibilities and Limitations of X-Ray Fluorescence spectrometry

With X-rays, electrons can be ejected from an atom. This leads to an atom with empty electronic states. The remaining shell electrons cascade downwards to reach the empty states. During this process, characteristic X-ray fluorescence radiation is emitted. This cascade

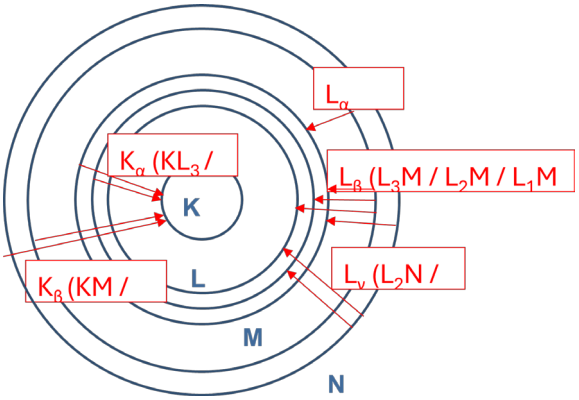

Figure 2: Sketch depicting the electronic transitions in an atom after an electron is lost because of an incident X-ray beam. The naming following the Siegbahn nomenclature (K_α, K_β, L_α, L_β, L_γ) is also used in the ELIO software. In parentheses, the transitions are given IUPAC nomenclature

can be seen in **figure 2**. Because the electric field of every chemical element is different, the X-ray fluorescence radiation exhibits energies that are characteristic for each chemical element, making it identifiable and quantifiable[17]. The intensities of these characteristic X-rays can be used to calculate the elemental composition of the sample under consideration[18]. However, for an accurate quantitative measurement both the attenuation of the incoming and outgoing radiation within the sample itself must be considered. Especially, fluorescence (outgoing) radiation might be absorbed again by another atom and thus cause secondary fluorescence, while at the same time the intensity of the primary radiation decreases. This results in a loss of accuracy for the measurement. **Figure 3** depicts a typical X-ray fluorescence spectrum obtained from a coin of the Claudius era. The coins of the Claudius and Nero era that were investigated are

[16] Vincze et al. 1993, 553–573; Vincze et al. 1995a, 1481–1500; Vincze et al. 1995b, 127–147; Vincze et al. 1999, 1711–1722; Schoonjans et al. 2012, 10–23; Schoonjans et al. 2013, 36–41.
[17] Moseley 1913, 1024–1034; Moseley 1914, 703–713.
[18] Broll 1986, 271–285.

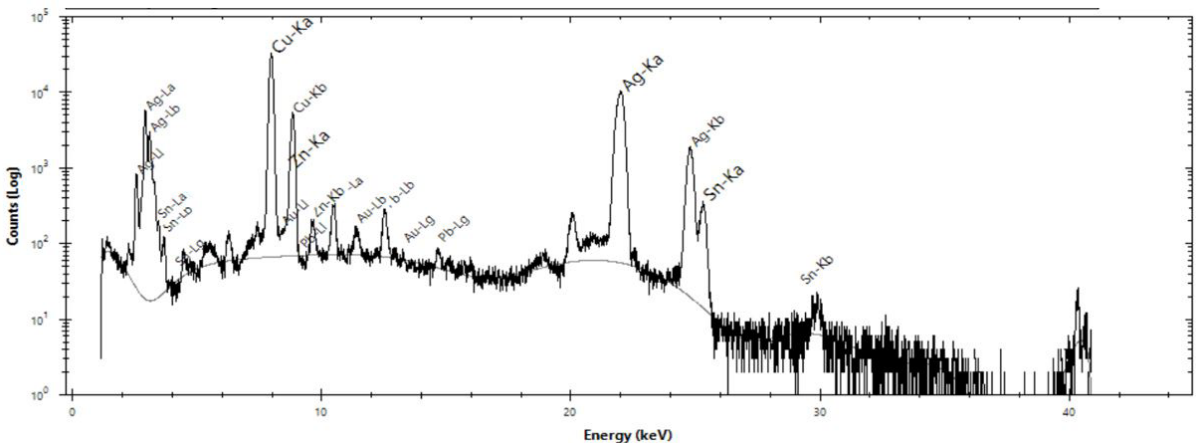

Figure 3: Spectrum of the characteristic X-ray fluorescence from the billon coin ALSK_0048. The spectrum shows clearly the presence of copper (Cu) and silver (Ag), as well as tin (Sn) and traces of zinc (Zn), gold (Au) and lead (Pb). The measurement time was 60 s with an ELIO SN1254 X-ray-spectrometer

billon coins, an alloy containing the main elements Cu and Ag. Visible in the spectrum are the K-Lines of Cu and Ag which are the most dominant. Furthermore K- and L-lines of other elements e.g. Au, Sn, Zn and Fe are also visible.

In general, XRF-spectrometry is an easy and fast method to investigate samples. A measurement time of only a few minutes already delivers meaningful results. This allows for a larger number of samples to be investigated with multiple measurements on each object thereby yielding a large set of statistical information. This means an increase in data precision. The obtained data enables, for instance, the classification of samples into distinct groups as well as the recognition of overarching trends among them.

1.4. Measurement of coins with portable XRF

Coins are generally suitable objects for XRF because they are made of characteristic metals or alloys. Elements with an atomic number lower than 11 (sodium, Na), which cannot easily be detected by XRF, are generally no main elements in coins. Although coins are a good example for a sample group containing many similar objects that can be compared on a statistical basis, XRF-measurements are done more commonly on paintings or papyrus inks. In those cases the analysis is simpler and therefore more accurate, because the above-mentioned self-attenuation in the sample can be neglected. This is due to the limited thickness of the paint in those objects. In contrast, the measurement of coins might not only be influenced by self-attenuation, but also by the presence of patina, or geometric effects (surface roughness) that must be considered. The penetration range of X-Rays may vary, depending on the X-Ray-source used but usually represents a penetration depth of 0.1 mm up to 1 mm. Therefore XRF-measurement data may not represent the core of a coin, but certainly the penetration depth of the X-Rays will be portrayed accordingly. The core of a coin may differ in its composition form the outer composite layers, but according to Ernst Gölitzer[19] a correlation between core material and outer layers seems plausible and would make vague assumptions about the overall material possible.

Patina effects on the measurement

Often coins build up a patina. Most materials are not resistant to oxidation or corrosion, thus forming a thin chemically modified surface layer. This patina might in general influence an XRF-measurement as the penetration depth of X-rays is typically on the scale of seve-

[19] Gölitzer 2004, 25–59.

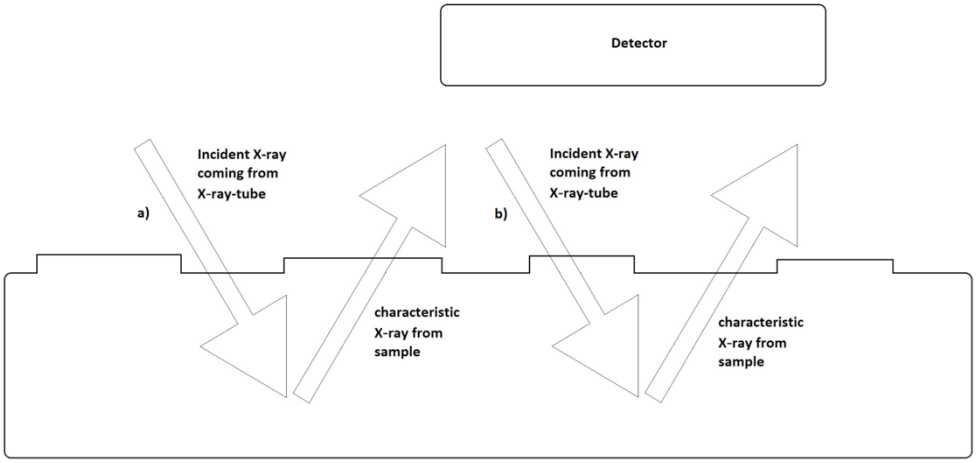

Figure 4: Sketch depicting the different pathways the characteristic X-rays take in an embossed coin. While in case a) the incident X-rays have a shorter path through sample material then the induced XRF, in case b) the situation is reversed

ral µm (depending on the element mixture of the sample and the exact energy of the X-rays). In principle, it is possible to correct measurements for patina effects[20]. But because the patina is mostly made up of oxides and therefore the density of that material is typically lower compared to the bulk material, the absorption of X-rays is lower in the patina than the rest of the coin. Especially when several objects can be compared on a statistical basis, patina effects play only a secondary role. Hence, exact determination of the elemental composition is challenging. A removal of the patina must be considered destructive and should therefore be avoided. However, as we will show below, in practical cases the patina might increase measurement uncertainty, but if several measurements are performed on the same object, these uncertainties can be quantified, and a comparison of objects is still possible. This means that the uncertainties resulting from a patina may be somewhat fixed in a statistical way by a large set of data, while a single data point will still be lacking in precision.

Self-absorption and secondary fluorescence

There are several influences on XRF-measurements. The size (solid angle) and the efficiency of the detector have an influence on the measurement, as well as the attenuation of the incident beam, the probability of photon creation, and the attenuation of the induced fluorescence radiation. As described above, additional X-ray fluorescence can be induced via secondary absorption inside the sample itself. The characteristic fluorescence of a heavy element can induce characteristic fluorescence of lighter elements in the sample, leading to an overrepresentation in intensity of the lighter elements compared to the heavier elements. Accuracy is negatively affected by secondary fluorescence. All these effects might be corrected collectively, in our works using either reference samples or computational simulation of XRF-measurements.

Surface irregularities

In addition to patina effects and self-absorption as well as secondary fluorescence, the geometric structure of the sample may influence the result of an analysis. The point is that the attenuation of the X-rays depends on the surface geometry (e.g. the embossment of the coins) of the samples. If the surface of the sample is structured, X-rays must travel through more or less coin material, depending

[20] Denker et al. 2005, 65–70.

on the incoming angle and outgoing angle of radiation (see **figure 4**).

Because different elements have different absorption coefficients and the penetration depth is also dependent on the energy the elemental X-rays have, the intensity of the X-ray can differ and lead to an additional uncertainty of the elemental composition. Although this behavior is difficult to treat in a mathematically exact way, we will show that the influence of this effect on the result can be estimated and can be partially overruled by performing several measurements on each sample, improving precision.

2. Experimental and Results

2.1. Coins under investigation

In this work, a total of 43 coins were measured with a portable ELIO SN 1254 XRF-spectrometer, 20 random lead-bronze coins from the Roman period and 23 billon coins (tetradrachms) issued under Claudius and Nero, respectively. Also, we chose silver coins for the second part of the paper, because silver coins from the early years of Claudius and Nero, between the reintroduction of silver coinage by Tiberius and the Neronian reform, have been underrepresented in literature so far. The main components of the lead-bronze coins are Cu, Sn and Pb; the main components of the billon coins are Cu and Ag. All coins stem from the coin collection of the Department of Classics of the University of Cologne and are listed in **table 1** according to their inventory numbers.

Lead-bronze coins	Billon coins Claudius	Billon coins Nero
AL_0039	ALSK_0047	AL_0187
AL_0093	ALSK_0048	AL_0188
AL_0417	ALSK_0058	AL_0189
AL_0537	ALSK_0059	ALSK_0169
AL_0563	ALSK_0060	ALSK_0170
AL_0609	AL_0061	ALSK_0171
AL_0654	AL_0062	
AL_0701	AL_0063	
AL_0815	AL_0064	
AL_0954	AL_0065	
AL_1179	AL_0075	
AL_1305	AL_0076	
AL_1359	AL_0081	
AL_1491	AL_0082	
AL_2210	AL_0086	
AL_2291	AL_0087	
AL_3375	AL_0088	
AL_3386		
AL_3404		
AL_3468		

Table 1: List of antique coins investigated with XRF in this work. Each coin has an identification number consisting of a letter code as well as a number code. The lead-bronze coins are listed in the first column (left) followed by the billon coins of Claudius (middle) and Nero (right)

2.2. Artificial reference samples

To derive correction factors for lead-bronze coins experimentally (see section 3.1.1 below), we produced 42 samples with known ratios (wt%) of Cu, Sn and Pb (see **table 2**). The ratios of the metals were selected such that they cover typical compositions of lead-bronze coins.

The amount of Cu varied from 70 to 95 wt%, reflecting the range of historical lead-bronze. The remaining wt% of the sample is split between Sn and Pb also in varying amounts. The powdered pure metals were weighed, mixed in their powdered form and melted for 3 hours without mechanical mixing at 1050 °C in graphite crucibles. This was done to ensure a homogenous melt to produce a coin-like form. It was verified by weighing that material loss due to evaporation was negligible. All in all, 42 different samples were produced. **Figure 5** below shows 4 of these reference samples.

Cu amount / wt%	Sn/Pb amount / wt%						
70	0/30	6/24	12/18	15/15	18/12	24/6	30/0
75	0/25	5/20	10/15	12.5/12.5	15/10	20/5	25/0
80	0/20	4/16	8/12	10/10	12/8	16/4	20/0
85	0/15	3/12	6/9	7.5/7.5	9/6	12/3	15/0
90	0/10	2/8	4/6	5/5	6/4	8/2	10/0
95	0/5	1/4	2/3	2.5/2.5	3/2	4/1	5/0

Table 2: Composition of the produced reference samples expressed as mass ratios of copper, tin and lead

	Copper (Cu)	Tin (Sn)	Lead (Pb)
Producer	Alfa Aesar	Acros Organics	Alfa Aesar
Purity	99%	99.5%	99.95%
Grain size	~100 Mesh	~100 Mesh	~100 Mesh

Table 3: Chemicals used to produce reference samples

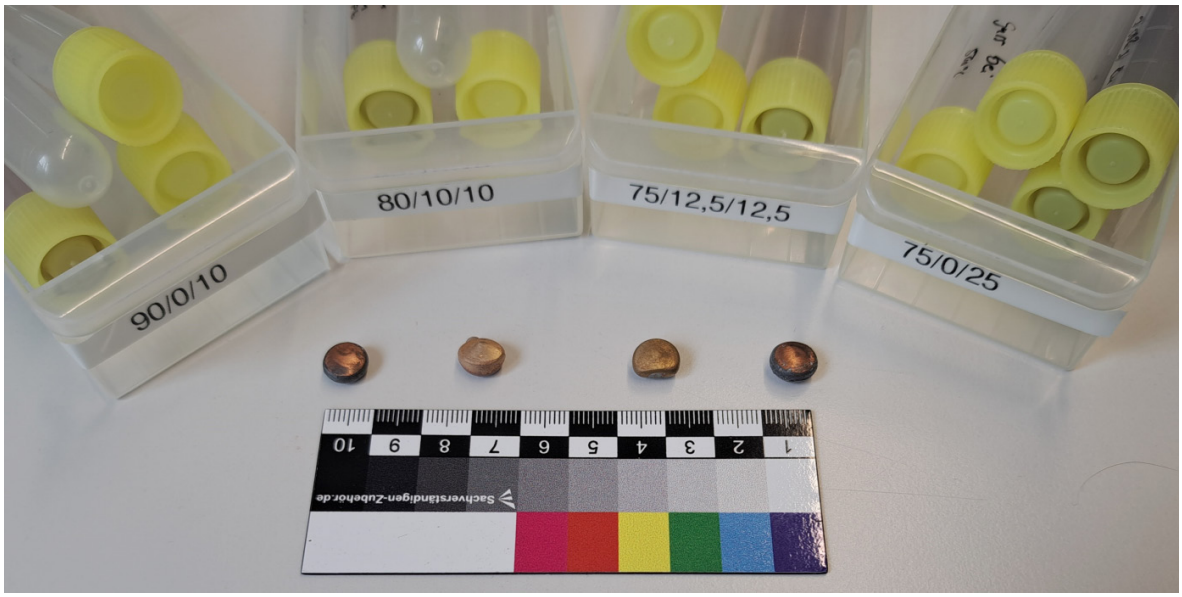

Figure 5: Four produced reference samples of lead-bronze coins used in this work

2.3. XRF measurements

To obtain a set of data for each coin that was measured, ten different measurements were done on each coin side. 8 measurements were taken along the rim of the coins and 2 measurements in the center. Measuring spots can be seen in **figure 6**.

The measurements of coins and reference samples were done with the ELIO device, and the composite analysis was done by the ELIO software. To obtain a more precise data set, only the expected or probable elements of these coins were investigated (i.e., selected as possible components in the analysis software). These were Cu, Ag, Pb and Sn as main components as well as Zn, Fe and Au as secondary components. The reference samples were measured in the same manner as the billon and lead-bronze coins.

Figure 6: Points of measurement on a coin sample (ALSK_0171, obverse)

3. Results and Discussion

3.1. Correcting measurement data based on reference samples

As described above, to correct the X-ray intensities of the different elements for self-attenuation and secondary fluorescence in coins (or general in thicker samples), correction factors are needed. Such factors can either be developed experimentally or from simulations. In this work both methods were used as described in the next paragraphs.

3.1.1. Correction factors (experimental)

A correction factor for the measurement of Pb/Cu in lead-bronzes was derived experimentally. This was done to enhance accuracy of XRF. The 42 reference samples (section 2.2.) were measured with XRF to deduce the impact of the different metals to each other. The measured mass fractions of Cu, Sn, and Pb of all 42 samples were plotted vs. the actual mass fractions (see **figure 7**). The measured fractions were taken from output of the ELIO software, averaged over 20 measurements as described above, to increase the precision of the data. The actual mass fractions were calculated from the weightings of the raw materials, see section 2.2. The dashed lines represent linear fits. While the tin mass fractions are very near to their nominal values, the lead and copper values deviate. The Pb concentration is obviously underestimated, and the Cu concentration is overestimated. This agrees with the assumption that secondary absorption plays an important role, because the fluorescence radiation of heavier elements might be absorbed again by lighter elements. Also, the deviation is linear within the given concentration range.

Therefore, a correction factor ($F_{Pb_{corr}}$) for the wt% value of lead can be calculated as the

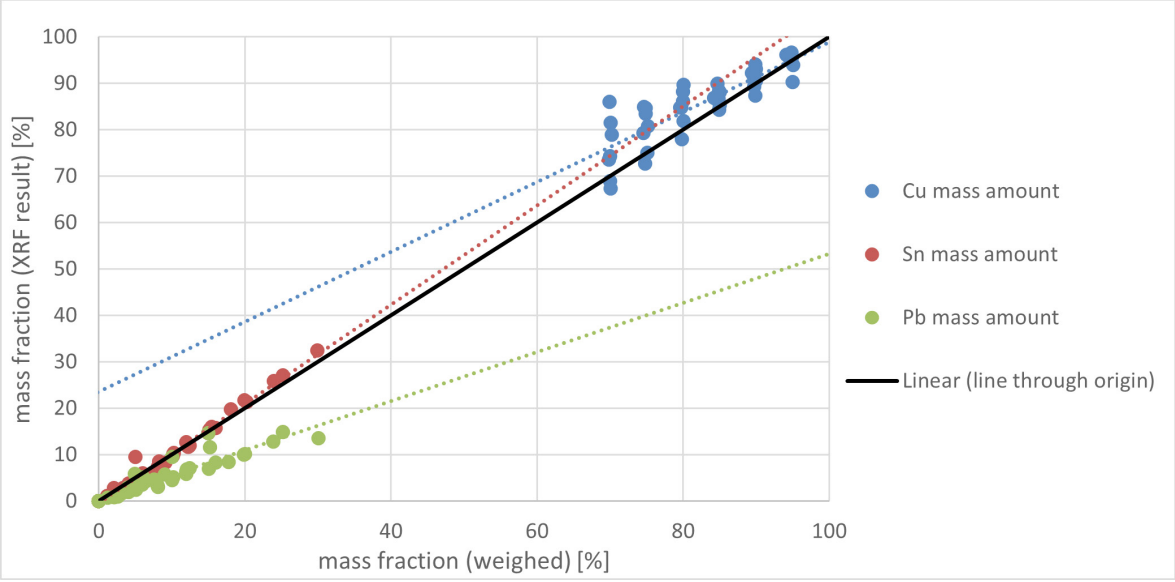

Figure 7: The amount of element measured versus the actual amount in the sample before correction with linear fits

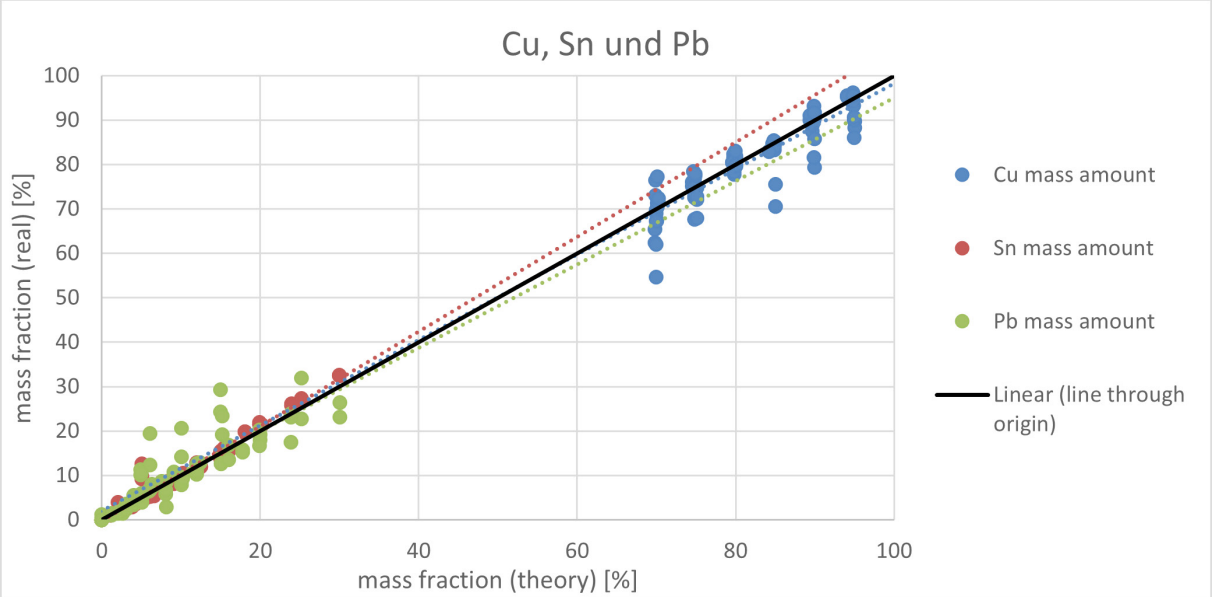

Figure 8: The amount of element measured versus the actual amount in the sample after correction

reciprocal slope of the linear fit shown in **figure 6**. This yields the following correction factor.

(1) $F_{Pb_{corr}} = 1.84 \pm 0.43$

To apply the correction, the nominal lead content (in %, ELIO software output) is multiplied by the correction factor. The resulting nominal elemental concentrations are then renormalized to 100%. If the resulting values for Cu, Sn, and Pb are plotted again (**figure 8**), it turns out that not only the Sn data are now fitting satisfyingly, but also the Cu data. All values are now close to the bisecting line. No second correction factor is needed in this ternary alloy. Obviously, lead is underestimated by the same factor as copper is overestimated. This agrees well with the assumption that the measurements are mainly affected by reabsorption of lead fluorescence radiation by copper and the subsequent secondary copper X-ray fluorescence. From our experience this correction factor is reliable within the range of sample compositions under investigation, which is all samples not containing more than 30 wt% lead, covering the typical compositions of lead-bronze coins.

3.2. Correction factor based on simulations

To obtain correction factors using a simulation, the experimental setup was modeled within the XMI-MSIM software. All parameters of the experiment were simulated, such as the properties of the X-ray-source, geometrical conditions, material and geometry of the sample, as well as material, size and form of the detector. For the simulations in this work, the X-ray source and detector were modeled as given in detail in the supplementary information. As samples, different billon coins were simulated with varying Cu/Ag ratios. As during XRF of coins, the X-ray beam is completely attenuated within the sample, the coins were modeled as infinitely thick layers within XMI-MSIM. The simulated sample furthermore contained 1.86 wt% trace elements like Pb, Zn, Sn, Au and Fe besides the two main elements Cu and Ag, which is a typical amount of trace elements for billon coins. The measurement geometry in the first simulation step was modeled after the geometry of the ELIO device. The resulting spectra were evaluated within XMI-MSIM, and a correction factor correcting the ratio of Ag and Cu was to be deduced by comparing via the simulated X-ray line intensities (details see

1	2	3	4	5	6
Cu / wt%	Ag / wt%	I(Cu) a.u.	$I(Cu)/(I(Cu)_{5\%})$	I(Ag) a.u.	$I(Ag)/(I(Ag)_{5\%})$
93.2	4.91	95134.3	1.69	3275.05	1.00
88.3	9.81	86182.3	1.61	6438.89	0.98
83.4	14.7	77981.4	1.54	9503.02	0.97
78.5	19.6	70728.2	1.49	12511.2	0.96
73.6	24.5	63926.3	1.43	15420.5	0.94
68.7	29.4	57644.4	1.39	18281.8	0.93
63.8	34.3	51849.7	1.34	21053.8	0.92
58.9	39.3	46384.8	1.30	23784.8	0.91
54.0	44.2	41322.9	1.26	26452.9	0.90
49.1	49.1	36512.7	1.23	29051.3	0.89
44.2	54.0	32033.5	1.20	31664.6	0.88
39.3	58.9	27709.6	1.17	34129.9	0.87
34.3	63.8	23676.2	1.14	36558.7	0.86
29.4	68.7	19837.3	1.11	38982.5	0.85
24.5	73.6	16135.8	1.09	41417.9	0.54
19.6	78.5	12621.9	1.06	43758.7	0.84
14.7	83.4	9284.38	1.04	46004.1	0.83
9.81	88.3	6066.77	1.02	48297.8	0.82
4.91	93.2	2971.09	1.00	50506.6	0.81

Table 4: Simulated billon alloys. Row 1: Cu content (wt%) of the simulated sample (simulation input). Row 2: Ag content (wt%) of the simulated sample (simulation input), Row 3: Intensity (peak area, simulation output) of Cu peak in the simulated spectra, Row 5: Intensity of Cu peak normalized to Intensity at 5% Cu content, Row 5: Intensity (peak area, simulation output) of Ag peak in the simulated spectra, Row 6: Intensity of Ag peak normalized to Intensity at 5% Ag content

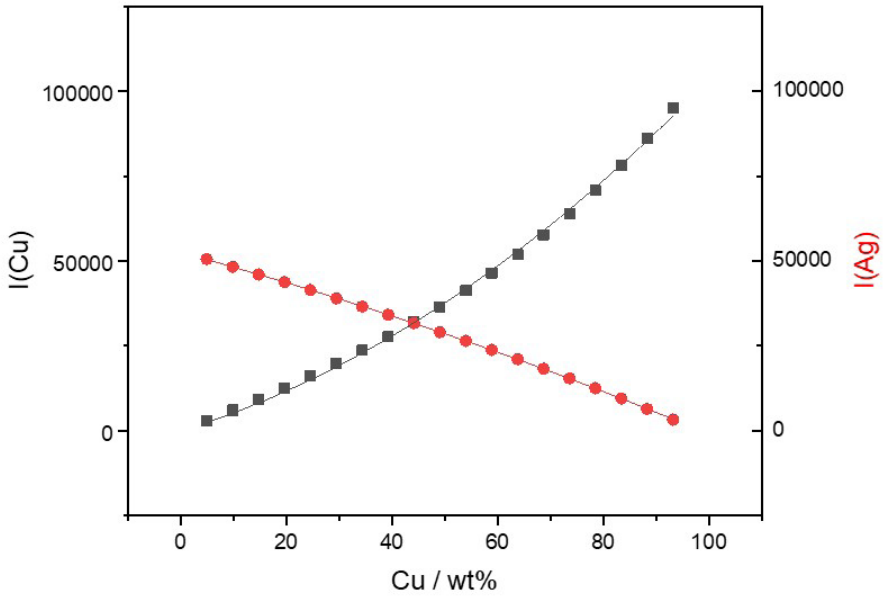

Figure 9: Intensities of Cu and Ag (rows 3 and 5 of **table 4**) plotted versus the amount of Cu in wt%

below). The amount of trace elements was the same at each simulation run, while only the ratio of Cu and Ag changed. This specific alloy composition was chosen to resemble the bulk of the tetradrachm coins measured via XRF.

The ratio of Cu and Ag varied from 95/5 to 5/95 in steps of 5 wt% for each element as can be seen in **table 4**. In **figure 9**, the intensities (peak areas) from the simulations are plotted vs. the nominal Cu content.

It is clearly visible that the intensities of Cu rise disproportionately with rising Cu content in the sample. The intensity of Ag radiation drops almost proportionately with rising Ag contents. Reason for this difference is probably the contribution of secondary X-ray fluorescence of Cu induced by the fluorescence radiation of Ag, reducing measurement accuracy. To correct this, a correction factor was derived from this data and can be seen in equations (2) and (3).

$$I_{corr} = \left(\frac{I_{5wt\%}}{I_{measured}}\right) I_{measured} \quad (2)$$

$$\left(\frac{I_{Cu}}{I_{Ag}}\right)_{corr} = F_{corr}\,\frac{I_{Cu}}{I_{Ag}} \quad (3)$$

At first all intensities were normalized to the intensity value of 5 wt% Cu or 5 wt% Ag respectively. By this, an influence factor can be obtained, which increases in the case of Cu with rising Cu wt% and decreases for Ag with rising Ag wt%. By multiplying the respective intensities with the reciprocal influence factor corrected Intensities were obtained. Then these corrected intensities were used to calculate corrected intensity ratios. The corrected values are given in **table 5**.

Plotting the corrected ratios over the simulated ratios yields a straight line through the origin (**figure 10**), indicating that all values can be transformed using the same correction factor over the whole concentration range. The correction factor (1) F_{corr} = 0.602 can directly be derived from the slope of the line in **figure 10**. This correction factor can be applied directly to the data from the ELIO device.

Cu / wt%	I(Cu)	Ag / wt%	I(Ag)	$[I(Cu) / I(Ag)]_{korr}$
93.2	56451	4.91	3275	17.2
88.3	53480	9.81	6550	8.16
83.4	50509	14.7	9825	5.14
78.5	47537	19.6	13100	3.63
73.6	44566	24.5	16375	2.72
68.7	41595	29:4	19650	2.12
63.8	38624	34.3	22925	1.68
58.9	35653	39.3	26200	1.36
54.0	32682	44.2	29475	1.11
49.1	29711	49.1	32751	0.907
44.2	26740	54.0	36026	0.742
39.3	23769	58.9	39301	0.605
34.3	20798	63.8	42576	0.488
29.4	17827	68.7	45851	0.389
24.5	14855	73.6	49126	0.302
19.6	11884	78.5	52401	0.227
14.7	8913	83.4	55676	0.160
9.81	5942	88.3	58951	0.101
4.91	2971	93.2	62226	0.0478

Table 5: Shown are the corrected intensities of copper and silver as well as the corrected ratio between copper and silver

This result shows that correction factors for XRF measurements can not only be developed via the experimental route using reference samples as written in section 3.1.1 but also by simulations.

3.3. Influence of sample geometry (embossing) of coins on the accuracy of the results

In the following section the influence of different angles of incident beam will be shown. To investigate this phenomenon the composition of the simulated coin was kept the same, while the angle of the incident beam was varied. The following **table 6** shows the different intensities of induced Cu and Ag X-rays as well as the ratio between these intensities. The simulated setup of the XRF-spectrometer stayed the same, meaning that the detector stayed in the same position regarding the X-ray-tube. This

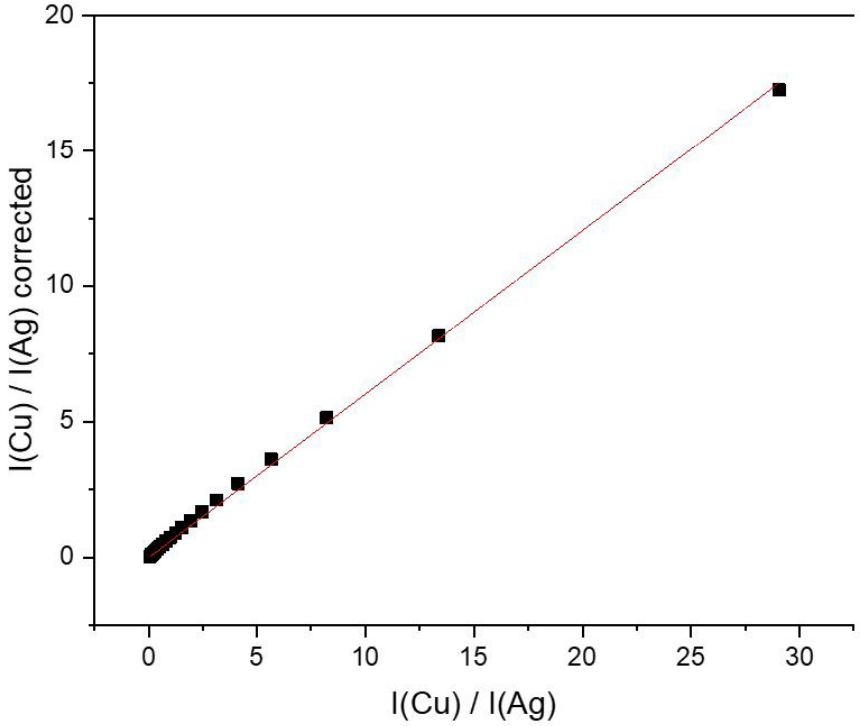

Figure 10: Plot of corrected ratio between copper and silver versus original ratio of copper and silver

leads to the detector changing its angle to the simulated sample with the X-ray-tube.

The ratio of intensities between Cu and Ag radiation changes with different angles of incident X-ray beam. This means that the elements Cu and Ag are affected in different ways by the different measurement geometries. Radiation with higher energy can pass more material than radiation with lower energy. This might be the reason the geometric effect is stronger for Cu than for Ag, because the Ag fluorescence has higher energies. The geometric effect will probably account for a large part of the uncertainties of single XRF measurements. This effect can be seen in the plot in **figure 11**.

Figure 11 shows the plot of Cu and Ag intensities over the angle of incident X-ray beam. The geometric effect is clearly visible with both elements but seems to be stronger for Cu than it is for Ag. With a very flat angle and the detector being almost perpendicular to the sample, this leads to a stronger overrepresentation of the element with lower energy

Angle of incident X-ray beam	I(Cu)	I(Ag)	I(Cu) / I(Ag)
-60°	52001	42424	1.23
-50°	47334	39666	1.19
-45°	45530	38542	1.18
-40°	43940	37485	1.17
-30°	41065	35657	1.15
-20°	38603	34014	1.13
-10°	36162	32372	1.12
0°	33773	30657	1.10
10°	31137	28747	1.08
20°	28127	26448	1.06
30°	24355	23443	1.04
40°	19154	18910	1.01
45°	15697	15586	1.01

Table 6: Intensities of copper, silver and the ratio between intensities of copper and silver I(Cu) / I(Ag)

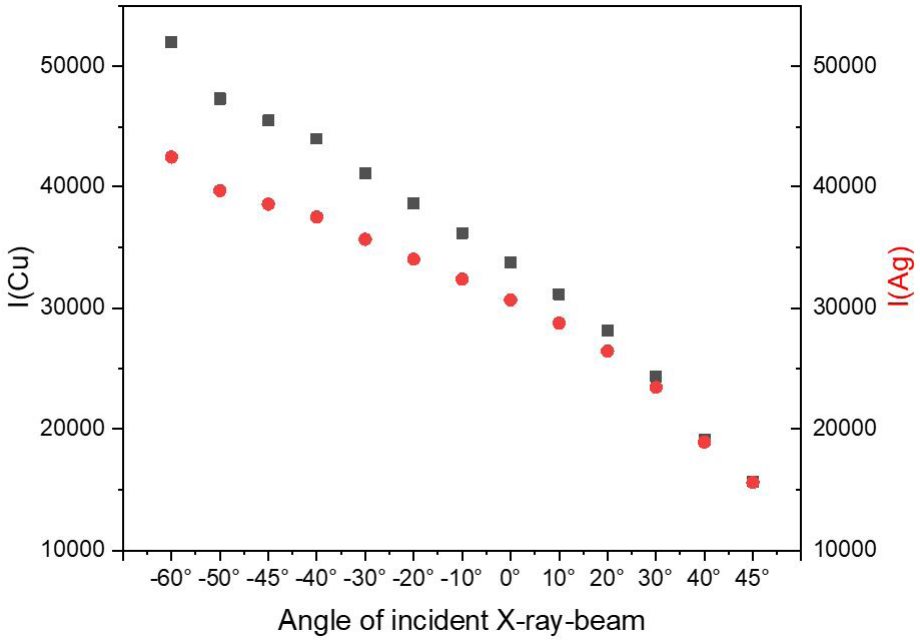

Figure 11: Intensity of copper (black) and silver (red) plotted against the angle of incident X-ray beam

radiation, because less thickness of the sample needs to be passed and the detector has an advantageous position. The general decline of intensity from -60° to +45° might come from the positioning of the detector to the sample. This result is of consequence in the case of irregular surfaces, like coins, as sketched in **figure 4**. Obviously, as documented in **table 6**, the influence of the exact surface geometry of a sample on the measured Cu/Ag ratio can be as much as 20%. This is comparable to the factual difference of measurements between two points of the same coin.

Thus, we conclude that the difference of measurement results from different points of the same coin is mainly caused by the surface geometry of the coins. In consequence, if a coin is measured with a portable XRF, it is good practice to measure several points and calculate average concentrations (as it is done throughout this work) to obtain more reliable (precise) results. The uncertainty of these average values will reflect the geometric effect described above.

3.4. Application of a correction factor in the investigation of billon coins

The billon coins were measured in the way mentioned in section 2.3. The obtained concentrations were adjusted applying the correction factor for Ag and Cu, respectively. Ten measurements per side of the coin were undertaken, totaling at 20 measurements for each coin. The results are given in **table 7**. On first sight, the compositions are typical billon materials within a narrow range of Cu/Ag ratios. Also, the data of the trace elements show no obvious trend. However, we plotted these data for each possible pair of elements. These plots were investigated via Pearsons's R, a statistical measure for the correlation of two components. This method is often used for handling large sets of data. A large set of data was collected to have more precise data. In this case we made use of Pearsons's R to identify possible links between different elements of the coins.

A value of 1 means a full positive correlation between two components, while a value of -1 indicates a full negative correlation. It turned out that most elements showed no correlation, except between Cu, Ag (the main

Sample	Cu/wt%	Ag/wt%	Au/wt%	Fe/wt%	Zn/wt%	Sn/wt%	Pb/wt%
Claudius							
ALSK_0047	2.88	95.38	0.41	0.06	0.03	0.62	0.63
ALSK_0048	29.14	69.31	0.28	0.06	0.19	0.53	0.49
ALSK_0058	46.51	51.62	0.32	0.11	0.49	0.6	0.35
ALSK_0059	59.8	38.22	0.36	0.1	0.66	0.64	0.21
ALSK_0060	36.42	61.96	0.27	0.15	0.28	0.52	0.4
AL_0061	63.66	34.07	0.26	0.13	0.88	0.42	0.58
AL_0062	47.03	51.28	0.28	0.1	0.48	0.62	0.2
AL_0063	30.52	67.35	0.38	0.1	0.28	0.73	0.64
AL_0064	68.59	29.35	0.18	0.15	0.86	0.49	0.39
AL_0065	42.74	54.59	0.42	0.18	1.32	0.41	0.33
AL_0075	64.9	33.25	0.23	0.15	0.77	0.39	0.32
AL_0076	68.33	29.77	0.22	0.12	0.78	0.34	0.45
AL_0081	30.07	68.28	0.4	0.08	0.55	0.41	0.21
AL_0082	67.46	30.66	0.36	0.1	0.84	0.37	0.21
AL_0086	58.39	39.69	0.13	0.12	0.85	0.52	0.31
AL_0087	53.01	41.99	0.45	0.41	3.55	0.32	0.27
AL_0088	36.72	60.56	0.27	0.08	0.8	0.58	0.99
Nero							
AL_0187	77.2	21	0.13	0.28	0.86	0.31	0.23
AL_0188	73.62	24.54	0.24	0.18	0.74	0.36	0.32
AL_0189	56.06	41.81	0.29	0.17	0.51	0.67	0.48
ALSK_0169	77.54	20.61	0.13	0.12	0.96	0.43	0.21
ALSK_0170	76.7	20.74	0.1	0.94	0.76	0.44	0.32
ALSK_0171	46.06	52.08	0.48	0.09	0.47	0.66	0.16

Table 7: Median values of each wt%-value for every element investigated for the billon coins

components) and the trace element Au (see **table 7**).

Pearson's R suggests that there are several correlations within the sample set. In principle such correlations could be used to differentiate between sample groups that are different due to production method, provenience, used raw materials, etc. The two main components of these coins are Cu and Ag. A fully negative correlation is to be expected and is also shown in Pearson's R with values of -0.999 and -0.998 respectively for both Claudius and the Nero coins. Interestingly, there is also a positive correlation between Ag and the trace element Au that can be seen from the data (and, consequently, a negative correlation between Cu and Au). Within the sample set of emperor Claudius, the correlation is smaller with a value of 0.403 than compared to the sample group of emperor Nero with 0.816 (see **figure 12**). The correlation between these two elements is evident in both sets of coins but is stronger (larger R value) for the coins of the Nero era. A correlation value of +1 would mean that every

Pearson's R	All billon coins	Nero	Claudius
Rxy/Cu(Ag)	-0.999	-0.999	-0.998
Rxy/Cu(Au)	-0.546	-0.817	-0.420
Rxy/Ag(Au)	0.534	0.816	0.403

Table 8: Pearson's R calculated for copper, silver and gold amounts of the analyzed samples

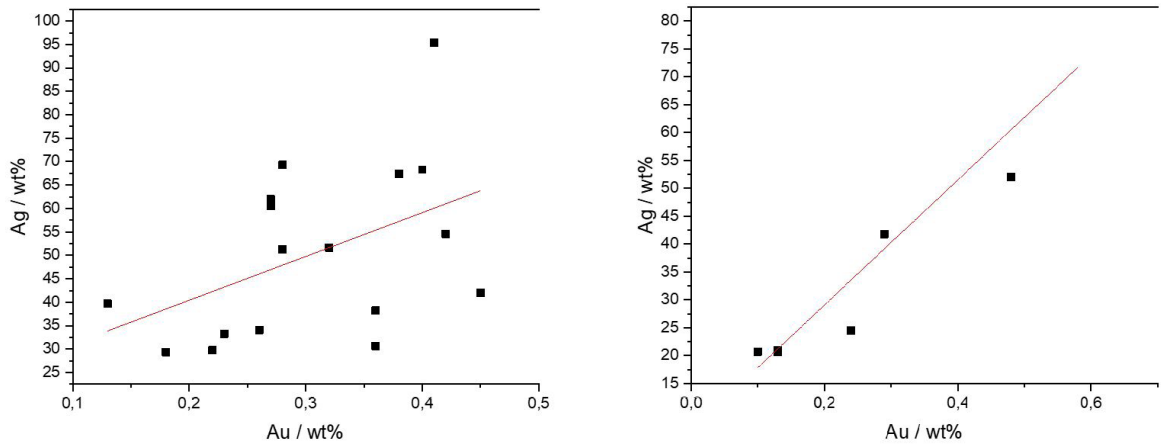

Figure 12: Plot of median values of gold and silver for the two subgroups of coins (Claudius left side / Nero right side)

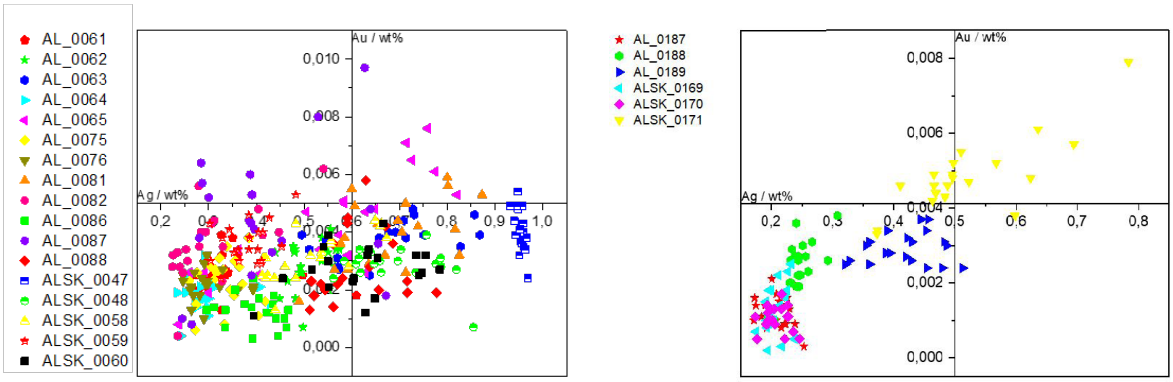

Figure 13: Plot of gold and silver amounts to determine the linear correlation between the two elements (Claudius left side / Nero right side). The different colors and shapes represent a data set of 20 measurements of one coin each

time a larger Ag value is measured, the Au value must also be larger. This is not the case for every measurement in our research, but this underlying trend was more often found in the Nero group as it was in the Claudius group, leading to the higher value for Pearson's R. The difference in correlation values may be an indicator to different origins of the metal ore, a different production site, or maybe recycling of some valuables into coins. But this would have to be reassured by other indicators as well.

While we have no immediate reason or interpretation at hand why these sample sets are different both groups can be divided from each other using this correlation as a criterion. This may be explained by the sample group, which is 2.5 times larger for Claudius than for Nero, which may result in a stronger correlation value.

Further, if not only the averaged Ag/Au concentrations of the coins are plotted but the individual measurements (color-coded in figure 13), it can be seen that the subset of Nero coins clearly shows a division into two clusters (**figure 13**, right side), where one group has lower silver and gold contents and the other group has larger silver and gold concentrations. Although there is some scattering of the single measurements, each coin falls clearly in one of these 2 clusters. An explanation for these different clusters must in any case lie in the different material compositions; more extensive serial examinations using this analytical method could perhaps develop further hypotheses about the different origins of the

raw materials or certain manufacturing mechanisms in the minting of the coins.

4. Conclusion

This work shows that the accuracy of data obtained through XRF-measurement can be improved by applying correction factors. Such correction factors can be obtained either by using reference samples as well as by simulations. A correction factor (1) F_{corr} = 0.602 for copper in billon coins was obtained from simulations with XMI-MSIM. With reference samples, a correction factor regarding the wt% amount of lead in lead-bronze coins was obtained. The value of this correctional factor is (1) $F_{Pb_{corr}}$ = 1.84. When these factors are multiplied with the nominal concentrations given by the ELIO software and the sum of all concentrations is renormalized to 100%, this yields also more precise Cu concentration. While the reference sample method is restricted to deliver a correction factor for a specific XRF-spectrometer and setup, the simulation-based approach can be adapted at much less expenditure to any measurement setup. Since the XRF measurements of coins showed a large variability of the compositions even when measuring the same coin at different spots, a simulation-based approach might be the preferred way to validly apply XRF methods on coins. However, any such correction will be specific for certain material composition; any integration into an automatic software like the ELIO evaluation is therefore probably not practical.

Simulations were also used to estimate the influence of sample surface geometry. It can be concluded that the variance of single measurements on the same coin can be interpreted as measurement effects due to irregular surfaces. This effect influences precision, but precision can be increased by a larger data set.

All in all, while the accuracy of portable XRF remains an issue, enough single measurements on the same object will yield sufficient precision to enable meaningful comparisons of coins, especially groups of coins. This might offer new insights on a set of coins and might open new perspectives if many samples (coins) are analyzed, which is relatively easy with portable XRF.

A drawback for measuring coins might be the fact that elemental composition of coins is not homogenous regarding core and outer shell. The works of Damian Gore and Gillan Davis[21] suggest that especially for Ag containing coins the composition between core and shell differs. On the outside the content is usually significantly higher than in its core. Also, Gore and Davis have suggested mathematical modelling for correcting the data given by XRF. This is further strengthened by Gölitzer[22]. But these works also indicate a correlation between Ag content of core and shell of a coin. This means if the outer shell of a coin is measured more precisely, also the core data becomes more precise as well. Of course, some accuracy is lost but for the comparison of coins and coin groups, accuracy is of less importance than precision. Gore compared XRF data with destructive techniques (ICP-MS) to verify his findings, also improving accuracy, but in our view, this is no prerequisite for the analysis of composition trends. Because XRF using portable spectrometers is possible within a museum environment and a single measurement is very fast (a few minutes), many samples and many measurements on one sample can be measurements, which is a unique advantage to other methods. The larger the datasets, the easier it is to identify groups or show (yet unknown) trends within groups. Even if other methods, especially destructible methods, yield more accurate results, this shows the advantageous application of relatively simple X-ray equipment. We would like to emphasize these strengths of portable XRF, underpinning e.g. previous examples referred to by Liritzis and Zacharias[23],

21 Gore – Davis 2016, 840–851; Davis et al. 2020.
22 Gölitzer 2004, 25–59.
23 Liritzis – Zacharias 2011, 109–142.

although other, partially more accurate and precise, analytical methods are at hand.

All in all, this work shows that especially when correction factors are applied, it is possible to use XRF successfully for the elemental characterization of coins. Correction factors are needed to obtain more accurate results, especially for the main components of the coins, while the analysis of trace amounts is not influenced as strongly. A sufficient number of single measurements with portable XRF improves precision sufficiently, providing easy access to measurement of high sample numbers with the potential to discover yet unknown trends in composition.

References

Alfeld 2020
M. Alfeld, MA-XRF for Historical Paintings: State of the Art and Perspective, Microscopy and Microanalysis 26, 2020, 72–75. DOI 10.1017/S1431927620013288

Boumans – Vrakking 1987a
P. W. J. M. Boumans – J. J. A. M. Vrakking, Detection Limit Including Selectivity as a Criterion for Line Selection in Trace Analysis Using Inductively Coupled Plasma-Atomic Emission-Spectrometry (Icp-Aes) – a Tutorial Treatment of a Fundamental Problem of Aes, Spectrochim Acta B 42, 1987, 819–840. DOI 10.1016/0584-8547(87)80144-1

Boumans – Vrakking 1987b
P. W. J. M. Boumans – J. J. A. M. Vrakking, Detection Limits of About 350 Prominent Lines of 65 Elements Observed in 50 and 27 Mhz Inductively Coupled Plasmas (Icp) – Effects of Source Characteristics, Noise and Spectral Bandwidth – Standard Values for the 50 Mhz Icp, Spectrochim Acta B 42, 1987, 553–579. DOI 10.1016/0584-8547(87)80034-4

Boumans – Vrakking 1987c
P. W. J. M. Boumans – J. J. A. M. Vrakking, Inductively Coupled Plasmas – Line Widths and Shapes, Detection Limits and Spectral Interferences – an Integrated Picture – Plenary Lecture, Journal of Analytical Atomic Chemistry 2, 1987, 513–525. DOI 10.1039/JA9870200513

Broll 1986
N. Broll, Quantitative x-ray fluorescence analysis. Theory and practice of the fundamental coefficient method, X-Ray Spectrometry 15, 1986, 271–285. DOI 10.1002/xrs.1300150410

Davis et al. 2020
G. Davis – D. B. Gore – K. A. Sheedy – F. Albarède, Separating silver sources of Archaic Athenian coinage by comprehensive compositional analyses, Journal of Archaeological Science 114, 2020, 105068. DOI 10.1016/j.jas.2019.105068

Denker et al. 2005
A. Denker – W. Bohne – J. Opitz-Coutureau – J. Rauschenberg – J. Röhrich – E. Strub, Influence of corrosion layers on quantitative analysis, Nuclear Instruments and Methods in Physics Research Section B: Beam Interactions with Materials and Atoms 239, 2005, 65–70. DOI 10.1016/j.nimb.2005.06.180

Gölitzer 2004
E. Gölitzer, Entstehung und Entwicklung des alexandrinischen Münzwesens von 30 v. Chr. bis zum Ende der julisch-claudischen Dynastie (Berlin 2004) 25–59. https://d-nb.info/970801572

Gordus et al. 1967
A. A. Gordus – W. C. Fink – M. E. Hill – J. C. Purdy – T. R. Wilcox, Identification of Geologic Origins of Archaeological Artifacts – Automated Method of Na and Mn Neutron Activation Analysis, Archaeometry 10, 1967, 87–96. DOI 10.1111/j.1475-4754.1967.tb00618.x

Gore – Davis 2016
D. B. Gore – G. Davis, Suitability of Transportable EDXRF for the On-site Assessment of Ancient Silver Coins and Other Silver Artifacts, Applied Spectroscopy 70, 2016, 840–851. DOI 10.1177/0003702816638283

Greenberg et al. 2011
R. R. Greenberg – P. Bode – E. A. D. Fernandes, Neutron activation analysis: A primary method of measurement, Spectrochim Acta B 66, 2011, 193–207. DOI 10.1016/j.sab.2010.12.011

Guerra et al. 2008
M. F. Guerra – M. Radtke – I. Reiche – H. Riesemeier – E. Strub, Analysis of trace elements in gold alloys by SR-XRF at high energy at the BAM, Nuclear Instruments and Methods in Physics Research Section B: Beam Interactions with Materials and Atoms 266, 2008, 2334–2338. DOI 10.1016/j.nimb.2008.03.008

Houk et al. 1980
R. S. Houk – V. A. Fassel – G. D. Flesch – H. J. Svec – A. L. Gray – C. E. Taylor, Inductively Coupled Argon Plasma as an Ion-Source for Mass-Spectrometric Determination of Trace-Elements, Analytical Chemistry 52, 1980, 2283–2289. DOI 10.1021/ac50064a012

Hoyo-Meléndez 2017
J. M. Del Hoyo-Meléndez, X-Ray Fluorescence (XRF) Spectrometry, in: B.-K. Anna – M. Lindsay (eds.), Digital Techniques for Documenting and Preserving Cultural Heritage (Amsterdam 2017) 257–262. DOI 10.2307/j.ctt1xp3w16

Jarvis – Williams 1993
K. E. Jarvis – J. G. Williams, Laser-Ablation Inductively-Coupled Plasma-Mass Spectrometry (La-Icp-Ms) – a Rapid Technique for the Direct, Quantitative-Determination of Major, Trace and Rare-Earth Elements in Geological Samples, Chemical Geology 106, 1993, 251–262. DOI 10.1016/0009 2541(93)90030-M

Johansson 1989
S. A. E. Johansson, PIXE: a Novel Technique for Elemental Analysis, Endeavour 13, 1989, 48–53. DOI 10.1016/0160-9327(89)90002-1

Johansson 1990
S. A. E. Johansson, Recent Progress in Particle Induced X-Ray-Emission Analysis (Pixe), Chemia Analityczna 35, 1990, 167–188.

Kusko et al. 1990
B. H. Kusko – M. Menu – T. Calligaro – J. Salomon, PIXE at the Louvre Museum, Nuclear Instruments and Methods in Physics Research Section B: Beam Interactions with Materials and Atoms 1990, 49, 288–292. DOI 10.1016/0168-583X(90)90262-S

Liritzis – Zacharias 2011
I. Liritzis – N. Zacharias, Portable XRF of Archaeological Artifacts: Current Research, Potentials and Limitations, X-Ray Fluorescence Spectrometry (Xrf) in Geoarchaeology 2011, 109–142. DOI 10.1007/978-1-4419-6886-9_6

Malmqvist et al. 1989
K. G. Malmqvist – L. Asking – H. C. Hansson – R. Hellborg – G. Hylten – E. M. Johansson – S. A. E. Johansson – P. Kristiansson – P. Larsson – N. E. G. Lovestam – B. G. Martinsson – J. Pallon – B. Svantesson – E. Swietlicki – U. A. S. Tapper – K. Themner, Pixe and Proton Microprobe Advances at the Lund-Institute-of-Technology, Nuclear Instruments and Methods in Physics Research Section B: Beam Interactions with Materials and Atoms 40-1, 1989, 685–689. DOI 10.1016/0168-583X(89)91075-6

Moseley 1913
H. G. J. Moseley, XCIII. The high-frequency spectra of the elements, The London, Edinburgh, and Dublin Philosophical Magazine and Journal of Science 26, 1913, 1024–1034. DOI 10.1080/14786441308635052

Moseley 1914
H. G. J. Moseley, LXXX. The high-frequency spectra of the elements. Part II, The London, Edinburgh, and Dublin Philosophical Magazine and Journal of Science 27, 1914, 703–713. DOI 10.1080/14786440408635141

Mozgai et al. 2021
V. Mozgai – B. Bajnóczi – Z. May – Z. Mráv, Non-destructive handheld XRF study of archaeological composite silver objects-the case study of the late Roman Seuso Treasure, Archaeological and Anthropological Sciences 13, 2021. Open Access: DOI 10.1007/s12520-021-01321-4

Pimentel 1960
G. C. Pimentel, Infrared spectroscopy: A chemist's tool, Journal of Chemical Education 37, 1960, 651. DOI 10.1021/ed037p651

Proctor – Yu 1950
W. G. Proctor – F. C. Yu, The Dependence of a Nuclear Magnetic Resonance Frequency Upon Chemical Compound, Physical Review 77, 1950, 717–717. DOI 10.1103/PhysRev.77.717

Reiche et al. 2004
Reiche – A. Berger – W. Görner – S. Merchel – M. Radtke – J. Riederer – H. Riesemeier – M. Roth, Following the traces of Albrecht Durer: analysis of silverpoint drawings by spatially resolved synchrotron-induced X-ray fluorescence analysis, Nuclear Instruments and Methods in Physics Research Section B: Beam Interactions with Materials and Atoms226, 2004, 83–91. DOI 10.1016/j.nimb.2004.03.081

Schoonjans et al. 2012
T. Schoonjans – L. Vincze – V. A. Solé – M. Sanchez del Rio – P. Brondeel – G. Silversmit – K. Appel – C. Ferrero, A general Monte Carlo simulation of energy dispersive X-ray fluorescence spectrometers – Part 5: Polarized radiation, stratified samples, cascade effects, M-lines, Spectrochimica Acta Part B: Ato-

mic Spectroscopy 70, 2012, 10–23. DOI 10.1016/j.sab.2012.03.011

Schoonjans et al. 2013
T. Schoonjans – V. A. Solé – L. Vincze – M. Sanchez del Rio – K. Appel – C. Ferrero, A general Monte Carlo simulation of energy-dispersive X-ray fluorescence spectrometers – Part 6. Quantification through iterative simulations, Spectrochimica Acta Part B: Atomic Spectroscopy 82, 2013, 36–41. DOI 10.1016/j.sab.2012.12.011

Shackley 2011
M. S. Shackley, X-Ray Fluorescence Spectrometry in Twenty-First Century Archaeology, in: M. S. Shackley (ed.), X-Ray Fluorescence Spectrometry (XRF) in Geoarchaeology (New York 2011) 1–6. DOI 10.1007/978-1-4419-6886-9_1

Vincze et al. 1993
L. Vincze – K. Janssen – F. Adams, A general Monte Carlo simulation of energy-dispersive X-ray fluorescence spectrometers – I: Unpolarized radiation, homogeneous samples, Spectrochimica Acta Part B: Atomic Spectroscopy 48, 1993, 553–573. DOI 10.1016/0584 8547(93)80060-8

Vincze et al. 1995a
L. Vincze – K. Janssens – F. Adams – K. W. Jones, A general Monte Carlo simulation of energy-dispersive X-ray fluorescence spectrometers Part 3. Polarized polychromatic radiation, homogeneous samples, Spectrochim Acta B 50, 1995, 1481–1500. DOI 10.1016/0584-8547(95)01361-X

Vincze et al. 1995b
L. Vincze – K. Janssens – F. Adams – M. L. Rivers – K. W. Jones, A general Monte Carlo simulation of ED-XRF spectrometers. II: Polarized monochromatic radiation, homogeneous samples, Spectrochimica Acta Part B: Atomic Spectroscopy 50, 1995, 127–147. DOI 10.1016/0584-8547(94)00124-E

Vincze et al. 1999
L. Vincze – K. Janssens – B. Vekemans – F. Adams, Monte Carlo simulation of X-ray fluorescence spectra: Part 4. Photon scattering at high X-ray energies, Spectrochimica Acta Part B: Atomic Spectroscopy 54, 1999, 1711–1722. DOI 10.1016/S0584-8547(99)00094-4

Van Ham-Meert et al. 2020
A. Van Ham-Meert – F. W. Rademakers – R. Gyselen – B. Overlaet – P. Degryse – P. Claeys, Sasanian copper and billon coins from the collections of the Royal Museums of Art and History, Brussels, Belgium-insights using semi-quantitative analysis by µXRF, Archaeological and Anthropological Sciences 12, 2020. DOI 10.1007/s12520-020-01191-2

Vittiglio et al. 1999
G. Vittiglio – K. Janssens – B. Vekemans – F. Adams – A. Oost, A compact small-beam XRF instrument for in-situ analysis of objects of historical and/or artistic value, Spectrochimica Acta Part B: Atomic Spectroscopy 54, 1999, 1697–1710. DOI 10.1016/S0584-8547(99)00100-7

Wallace et al. 2021
S. Wallace – N. Smith – N. Nerantzis, Handheld methods in archaeological research on large copper alloy assemblages: HH-XRF against HH-LIBS, Archaeometry 63, 2021, 343–371. DOI 10.1111/arcm.12595

Zmuda-Trzebiatowska et al. 2019
I. Zmuda-Trzebiatowska – J. M. del Hoyo-Meléndez – G. Sliwinski, Material composition evaluation of historical Cu alloy aquamanilia by complementary XRF and LIBS measurements, The European Physical Journal Plus 134, 2019. DOI 10.1140/epjp/i2019-12705-0